Measurements of Magnetic Properties of Kilogram-Level Test Masses for Gravitational-Wave Detection Using a Torsion Pendulum

Hang Yin,[1] Ding-Yin Tan,[1] Ming Hu,[2] Shun Wang,[1] Yan-Zheng Bai,[1] Shu-Chao Wu,[1] and Ze-Bing Zhou[1,*]

[1] *MOE Key Laboratory of Fundamental Physical Quantities Measurement, Hubei Key Laboratory of Gravitation and Quantum Physics, School of Physics, Huazhong University of Science and Technology, Wuhan 430074, People's Republic of China*

[2] *Institute of Geodesy and Geophysics, Chinese Academy of Sciences, Wuhan 430074, People's Republic of China*

In spaceborne gravitational-wave detectors, the stringent requirements on the magnetic cleanliness of the test masses (TMs) make the development of ground-based characterization techniques of their magnetic properties important. An electrostatically controlled torsion pendulum has been built to measure the magnetic properties of TianQin-like solid TMs. The remanent magnetization m_r and the magnetic susceptibility χ of TMs can be measured at the level of 1 nA m² and 8×10^{-7}, respectively. The precisions of measurements are mainly limited by the mechanical sensitivity of silicon fiber. The experimental results from a solid tungsten TM as an example show that the apparatus provides a feasible way to investigate the bulk effect of a full-size TM for the TianQin mission with enough resolution.

I. INTRODUCTION

Gravitational waves are a prediction of Einstein's general theory of relativity. They not only offer an important way to research the foundations of general relativity, but also they are expected to provide a method to explore the Universe. Aiming to observe gravitational waves in the millihertz frequency range, several missions for spaceborne gravitational-wave observatories have been proposed. Notably, these missions include LISA [1], OMEGA [2], LAGRANGE, and TianQin [3]. TianQin is a proposal for gravitational-wave detection in space in the millihertz frequency range, which is comprised of three Earth-orbiting spacecrafts in a nearly equilateral triangle formation. In TianQin, there are two "free-falling" cubic test masses (TMs) inside each spacecraft and the displacements of the spacecrafts are monitored by laser interferometry. The scientific goal of TianQin depends crucially on the purity of TM geodesic motion at low frequencies, which requires that the acceleration noise of the inertial sensors must be below 10^{-15} m/s² Hz$^{1/2}$ [3]. This motion is achieved by the drag-free control of the spacecrafts, where environmental disturbances are reduced by micronewton thrusters driven by position sensors. For LISA, it has been shown that the magnetic field of space plasma is the main source of the nonconservative forces exerted on the TMs [4–6]. The forces exerted by magnetic

field also play a significant role in TianQin, especially considering its geocentric orbit. The magnetic force on the TM can be expressed as

$$f = \iiint_V \nabla \left(\vec{m}_r \cdot \vec{B} + \frac{\chi}{2} \vec{H} \cdot \vec{B} \right) dx\, dy\, dz, \quad (1)$$

where m_r is the remanent magnetization of the TM, χ is the volume susceptibility of the TM, H is the environmental magnetic field strength, and B is the magnetic induction. The magnetic force comes from both the coupling between fluctuations of magnetic field strength and magnetic field gradient.

For spaceborne gravitational wave detections, fluctuations of magnetic field are expected to be dominated by the interplanetary magnetic field, and fluctuations of the magnetic field gradient are mainly due to the spacecraft itself. In order to realize scientific goals, the TMs must achieve the designed low susceptibility and at the same time retain high density to minimize the displacement caused by environmental force disturbance. The TM of LISA is made of gold-platinum alloy. The scientific goal of TianQin is similar to that of LISA. However, the sensitivity of TianQin's laser interferometer is lower than that of LISA because of its shorter laser arm. Therefore, the requirement for inertial sensor sensitivity must achieve 1×10^{-15} m/s²/Hz$^{1/2}$, which is higher than LISA's requirement. As a result, many more stringent requirements are demanded in TianQin's inertial sensor, including magnetic properties. In the TianQin mission, the requirements for the TMs are

_____
*zhouzb@mail.hust.edu.cn

proposed as total remanent magnetization $m_r < 10$ nA m^2 and volume susceptibility $\chi < 1 \times 10^{-6}$ [3,7], which are stricter than the requirements of LISA of $m_r < 20$ nA m^2 and $\chi < 3 \times 10^{-6}$ [8,9]. In the LISA pathfinder mission, the susceptibility and magnetic moment of TM have been measured to be $< 2.5 \times 10^{-5}$ [10] and < 4 nA m^2 [11]. Although the effects caused by low-frequency magnetic fluctuations are not expected to contribute significantly to noise projection, several force noise sources coupling to the bulk of the TM still cannot be excluded to date [12]. On the other hand, TianQin is a combination of three Earth-orbiting spacecraft in a nearly equilateral triangle formation. It is different from the LISA mission, which will be operated in heliocentric orbit. Compared to the LISA mission, the influence from background magnetic field is still non-negligible for the TianQin mission. LISA pathfinder shows that the development of TMs with low remanent magnetization and susceptibility demands ground-based experimental methods for measuring the magnetization of a sample of several centimeters in size in a laboratory. A superconducting quantum interference device, which is a typical magnetometer with high precision, has been used to measure the magnetic moment of TM in LISA pathfinder [13]. As is known, the influence of magnetic effect on an inertial sensor is embodied in magnetic torque. So the magnetic effect will be described more exactly by measuring directly the magnetic torque on a TM. However, the traditional torque magnetometry using a cantilever lacks sufficient sensitivity. Therefore, in this report we present a scheme based on a torsion pendulum to measure the magnetic properties of a solid TM. The magnetic susceptibility and remanent magnetization of a solid tungsten cubic TM are measured to demonstrate the sensitivity of the apparatus. Compared with the traditional torque magnetometer, replacing the cantilever with a torsion pendulum further improves the resolution of the measurement [14,15].

In the past two decades, torsion pendulums with suspended hollow cubic or lightweight TMs have been verified as an effective tool for investigating various surface effects of TM for the LISA mission by the University of Trento [16–18], University of Washington [19], University of Naples [20], and Huazhong University of Science and Technology [21–23]. However, the magnetic effect is a bulk effect and cannot be evaluated by suspending a hollow TM as before. In our scheme, an electrostatically controlled single-stage torsion pendulum suspending a solid cubic "massive" TianQin-like TM is established for the purpose of experimental study of magnetic properties on the ground.

II. MEASUREMENT PRINCIPLE

The magnetic susceptibility and remanent magnetization of a TM are obtained by measuring the magnetic torque exerted on the TM. A solid tungsten cubic TM is
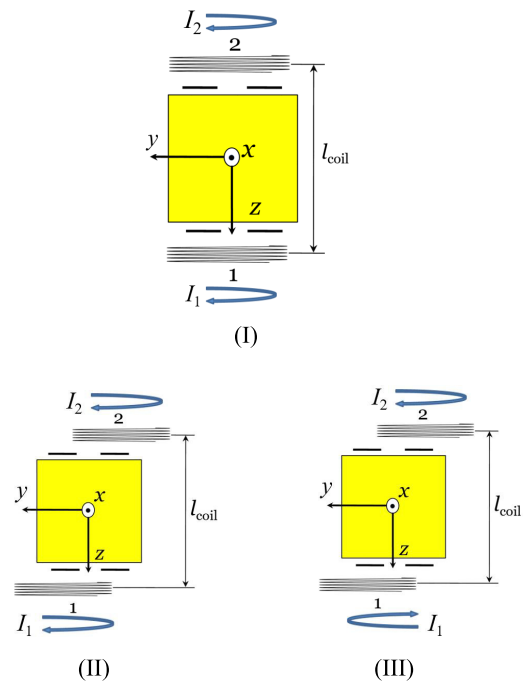

FIG. 1. Schematic view of symmetric and asymmetric setup of two circular magnetic coils (coil 1 and coil 2).

suspended by a silicon fiber and positioned between two circular magnetic coils, placed symmetrically or asymmetrically along a common z axis. In terms of the installation positions and current directions of the magnetic coils, there are three configurations used in the measurement process, as shown in Fig. 1. The three parameters, namely the remanent magnetization m_y, m_z and susceptibility χ, are obtained by measuring the magnetic torque in the three configurations independently.

The magnetic coils are made by wrapping enameled wires around aluminum plates, with an equivalent radius R of (1.7 ± 0.1) cm. Distance l_{coil} represents the distance between coil 1 and coil 2. In coordinates of Fig. 2, the centers of coil 1 and coil 2 are assigned as $(0, y_{o1}, z_{o1})$ and $(0, y_{o2}, z_{o2})$, respectively.
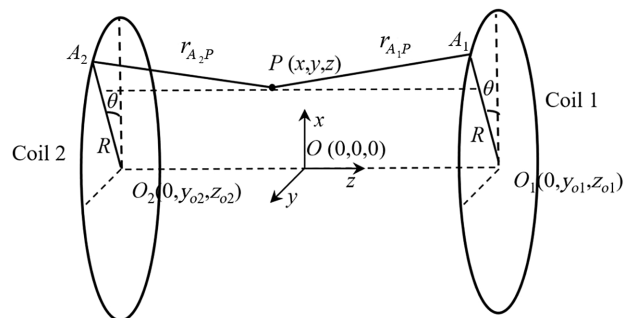

FIG. 2. Schematic diagram of magnetic field strength calculation on point $P(x, y, z)$.

According to the Biot-Savart law and ignoring spatial medium, the magnetic field at position $P(x,y,z)$ is expressed as follows:

$$
B_x = \frac{N\mu_0}{4\pi} \int_0^{2\pi} R\cos\theta \left(\frac{I_2(z-z_{o2})}{|r_{AP,2}|^3} + \frac{I_1(z-z_{o1})}{|r_{AP,1}|^3} \right) d\theta,
$$

$$
B_y = \frac{N\mu_0}{4\pi} \int_0^{2\pi} R\sin\theta \left(\frac{I_2(z-z_{o2})}{|r_{AP,2}|^3} + \frac{I_1(z-z_{o1})}{|r_{AP,1}|^3} \right) d\theta,
$$

$$
B_z = \frac{N\mu_0}{4\pi} \int_0^{2\pi} R \left(\frac{\frac{I_2(\sin\theta(y_{o2}-y)+R-\cos\theta x)}{|r_{AP,2}|^3}}{+ \frac{I_1(\sin\theta(y_{o1}-y)+R-\cos\theta x)}{|r_{AP,1}|^3}} \right) d\theta,
$$

$$\tag{2}$$

where $I_{1(2)}$ represents the current in coil 1(2), N is the number of turns of wires in each coil, and θ is the angle between $OA_{1(2)}$ and the x axis. The distance between $P(x,y,z)$ and a point on coil 1 or coil 2, represented by $r_{AP,1}$ and $r_{AP,2}$, is written as

$$
|r_{A_1 P}| = \sqrt{(x-R\cos\theta)^2 + (y-R\sin\theta-y_{o1})^2 + (z-z_{o1})^2},
$$

$$
|r_{A_2 P}| = \sqrt{(x-R\cos\theta)^2 + (y-R\sin\theta-y_{o2})^2 + (z-z_{o2})^2}.
$$

$$\tag{3}$$

The torsion pendulum has one degree of freedom, meaning only the torque along the vertical x axis can be detected, which can be written as

$$
\tau = \tau_{\text{grad}} + \tau_m, \tag{4}
$$

where τ_{grad} describes the torque caused by magnetic gradient and τ_m describes the interaction between the remanent magnetization $\vec{m}$ and the total applied magnetic field B. When m_ρ is used to express magnetization per unit volume, τ_{grad} and τ_m can be expressed, respectively, as Eqs. (5) and (6):

$$
\tau_{\text{grad}} = \iiint_{v_{\text{TM}}} \left(\vec{r} \times \vec{f} \right) dx\,dy\,dz
$$

$$
= \iiint_{v_{\text{TM}}} (yf_z - zf_y)dx\,dy\,dz, \tag{5}
$$

$$
\tau_m = \iiint_{v_{\text{TM}}} \left(\vec{m}_\rho \times \vec{B} \right) dx\,dy\,dz
$$

$$
= \iiint_{v_{\text{TM}}} (m_{\rho,y}B_z - m_{\rho,z}B_y)dx\,dy\,dz, \tag{6}
$$

where v_{TM} is the volume of the TM. The magnetic forces per unit volume f_z and f_y can be expressed as

$$
f_y = \left(\vec{m}_\rho + \frac{\chi}{\mu_0}\vec{B} \right) \frac{\partial \vec{B}}{\partial y}, \tag{7}
$$

$$
f_z = \left(\vec{m}_\rho + \frac{\chi}{\mu_0}\vec{B} \right) \frac{\partial \vec{B}}{\partial z}. \tag{8}
$$

In our calculation, we assume that the distribution of magnetic moment is uniform in the TM. The spatial distribution and strength of magnetic field can be adjusted by changing the position of coils and current intensity, leading to different magnetic torque on the TM. With I_1 and I_2 running in the same direction and magnetic coils installed asymmetrically, the magnetic torque acting on the TM is written as

$$
\tau = \tau_{\text{grad}} + \tau_m
$$

$$
= \iiint_{v_{\text{TM}}} \left[\begin{array}{c} \left(\frac{m_y}{v_{\text{TM}}} + \frac{\chi}{\mu_0}B_y \right)\left(y\frac{\partial B_y}{\partial z} - z\frac{\partial B_y}{\partial y} \right) \\ + \left(\frac{m_z}{v_{\text{TM}}} + \frac{\chi}{\mu_0}B_z \right)\left(y\frac{\partial B_z}{\partial z} - z\frac{\partial B_z}{\partial y} \right) \\ + \left(\frac{m_y}{v_{\text{TM}}}B_z - \frac{m_z}{v_{\text{TM}}}B_y \right) \end{array} \right]
$$

$$
\times dx\,dy\,dz. \tag{9}
$$

When two magnetic coils are installed asymmetrically with I_1 and I_2 running in opposite directions, the torque produced by the remanent magnetization can be ignored because of the centrosymmetric magnetic field. Only the torque produced by magnetic field gradient is present and the torque on the TM can be written as

$$
\tau' = \tau_{\text{grad}}
$$

$$
= \iiint_{v_{\text{TM}}} \left[\begin{array}{c} \left(\frac{m_y}{v_{\text{TM}}} + \frac{\chi}{\mu_0}B_y \right)\left(y\frac{\partial B_y}{\partial z} - z\frac{\partial B_y}{\partial y} \right) \\ + \left(\frac{m_z}{v_{\text{TM}}} + \frac{\chi}{\mu_0}B_z \right)\left(y\frac{\partial B_z}{\partial z} - z\frac{\partial B_z}{\partial y} \right) \end{array} \right]
$$

$$
\times dx\,dy\,dz. \tag{10}
$$

Otherwise, when the coils are installed symmetrically, with currents I_1 and I_2 running in the same direction, $\iiint_{v_{\text{TM}}} B_z dx\,dy\,dz$ is close to 0 T and the $m_y B_z$ term in Eq. (9) becomes dominant. The magnetic torque acting on the TM can be simplified as

$$
\tau'' = \tau_m = \frac{m_y}{v_{\text{TM}}} \iiint_{v_{tm}} B_z dx\,dy\,dz. \tag{11}
$$

If two coils cannot be installed perfectly symmetrical, an extra magnetic torque will be produced because of very small magnetic gradient. Therefore, the error δd_y shown in Fig. 3 should be less than 50 μm so that the error of remanent magnetization m_y is less than 0.2 nA m^2.

According to the analysis mentioned above, Eqs. (9)–(11) describe the magnetic torque in the different configurations shown in Fig. 1. Finally, two components of the
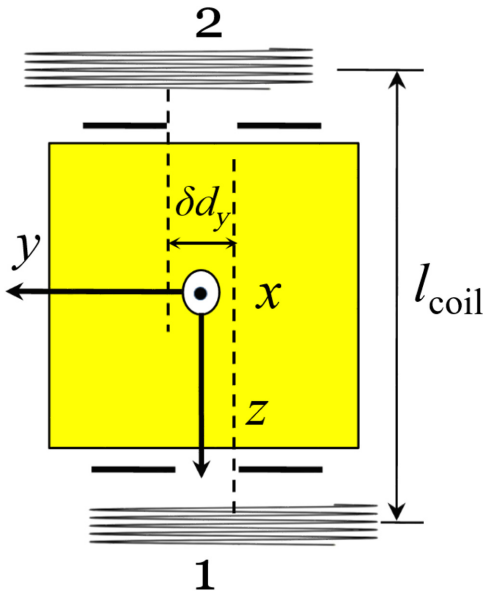
FIG. 3. Schematic view of the installation errors of magnetic coils.

FIG. 5. Noise power spectral density of the electrostatically controlled torsion pendulum. The black curve is the total noise of our facility. The blue curve is the action noise of the electrostatically controlled torsion pendulum. The red line is the theoretical thermal noise of fiber with a quality factor of 275 000.

test mass remanent magnetization, namely m_y and m_z, and the magnetic susceptibility χ can be obtained by solving Eqs. (9)–(11).

III. EXPERIMENTAL FACILITY AND RESULTS

A schematic diagram of a single-stage torsion pendulum is shown in Fig. 4, which includes the TM, two pairs of electrodes, and magnetic damping. Here, the magnetic properties of a tungsten cube TM, with a size of $(4 \times 4 \times 4)$ cm^3 and a mass of 1.23 kg, are measured to demonstrate the sensitivity of the apparatus. In the future, TMs with lower magnetic susceptibility for TianQin will also be measured using this facility. The TM is suspended by a silica fiber (silica fiber 2) of 40 cm in length and 310 μm in diameter. Another silica fiber (silica fiber 1), which is 5 cm long and 400 μm in diameter, is used to
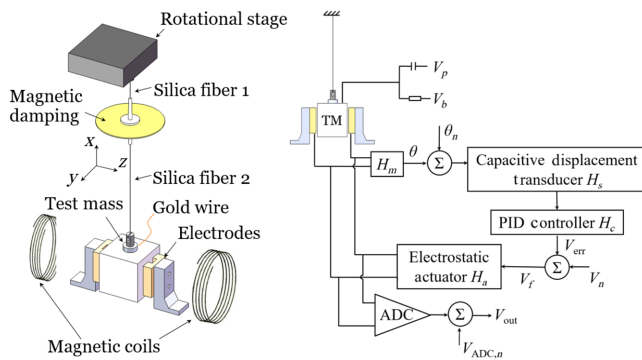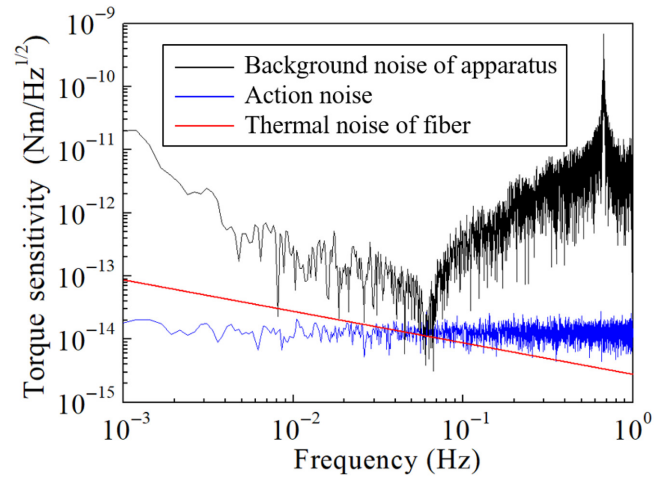

FIG. 4. Schematic view of the torsion pendulum apparatus and control block diagram.

connect the rotational stage with the magnetic damping. In this torsion pendulum the TM is connected to the silica fiber by a very small connector and glue so that the test mass does not lead to any modification in measurement. The resonant frequency of the torsion pendulum is 0.07 Hz. In order to linearize the electrostatic actuator and drive the capacitive transducer, a thin gold wire with a diameter of 10 μm is connected to the TM to apply a dc voltage V_b and a 50 kHz pumping voltage V_p. The mechanical behavior of the gold wire can be ignored because of its much smaller stiffness compared with the silica fiber. Two pairs of aluminum electrodes as a part of a capacitive sensor are mounted on both sides of the TM to monitor the motion of the TM, to guide a controller to generate appropriate voltages applied to the electrodes. The whole apparatus is in a vacuum chamber with a vacuum level of 3×10^{-5} Pa.

During the measurement process, the TM is kept still, with the magnetic torque τ balanced by the feedback torque τ_f provided by a capacitive transducer at a capacitive noise level of 2×10^{-7} pF/Hz$^{1/2}$ [24]. The value of τ is obtained by calculating the feedback torque τ_f from the applied voltages. Shown in Fig. 5, the torque noise floor of the electrostatically controlled torsion pendulum reaches 2×10^{-14} Nm/Hz$^{1/2}$ at its resonant frequency, limited by the thermal noise of fiber and the actuation noise with a level of 2 μV/Hz$^{1/2}$ [25].

Figure 6 shows photographs of the two configurations where two magnetic coil panels, perpendicular to the z axis, are installed on both sides of the TM symmetrically and asymmetrically. The gap l_{coil} between the coils is (12.5 ± 0.1) cm and the total number of turns N of each coil is 240. The symmetrically installed coils with dc current $I_1 = I_2 = 1.5$ A produce magnetic field with strength
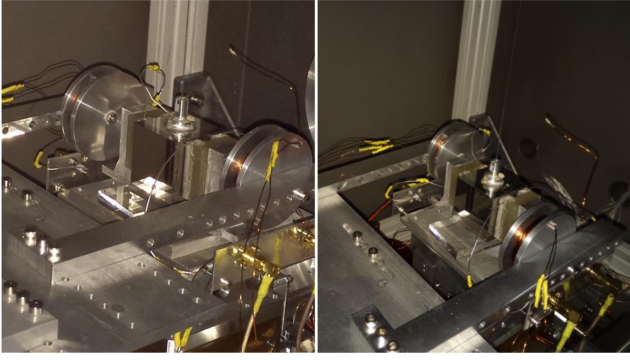
FIG. 6. Photos of the apparatus. Two magnetic coils are installed in the symmetric (left) and the asymmetric (right) configuration.

of $B_z = 460$ μT near the center of the TM. To verify the correctness of the calculated magnetic field from Eq. (2), the magnetic intensity is measured by a magnetometer at more than 27 different locations between the two coils. The measured data and the theoretical calculation coincide within a maximum difference of 3.7%. Taking one point $(-1.5, -2.2, -0.25)$ as an example, the measured curve and theoretical curve of magnetic field with different currents of 0.05, 0.1, 0.15, 0.2, and 0.25 A are shown in Fig. 7. According to the power spectral density of the apparatus and errors of installations, the main errors are listed in Table I. A time switch is used to produce a square-wave oscillating current so as to change magnetic field periodically. As shown in Fig. 8, when both of the symmetric coils are loaded with the same square-wave oscillating currents of fixed period of 300 s, the variational feedback torque is $\Delta\tau_f = \Delta\tau'' = -(1.43 \pm 0.03) \times 10^{-11}$ Nm. According to Eq. (11), variation of magnetic field strength $\iiint_{v_{TM}} B_y \, dx \, dy \, dz / v_{TM}$ is 451 μT, corresponding to a current variation from 0 to 1.5 A. Therefore, the remanent magnetization along the y axis is calculated to be $-(31.70 \pm 0.71)$ nA m^2.

In the asymmetric configuration, the distance between the two magnetic coils is (40.30 ± 0.05) mm along the y axis. When the currents loaded in both coils have the same direction, period, and amplitude, the magnetic torque τ has two components τ_{grad} and τ_m. The variation of
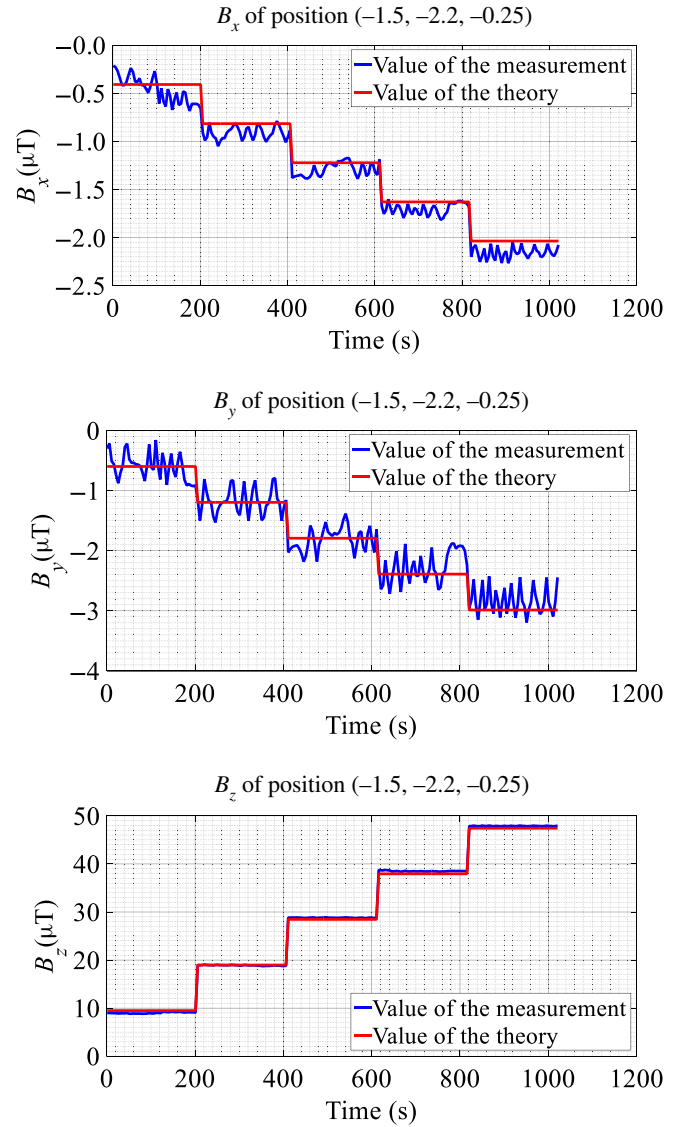

FIG. 7. Curves of magnetic field are measured by a magnetometer (blue curves) and calculated by theoretical model (red curves) when different currents are loaded in the magnetic coils.

magnetic torque on the TM $\Delta\tau$ is $(2.79 \pm 0.07) \times 10^{-11}$ Nm when the peak-to-peak value of the currents is 1.5 A. On the other hand, when the directions of the currents are opposite, the magnetic torque τ' is only caused

TABLE I. Error budget (integral time is 3 hours).

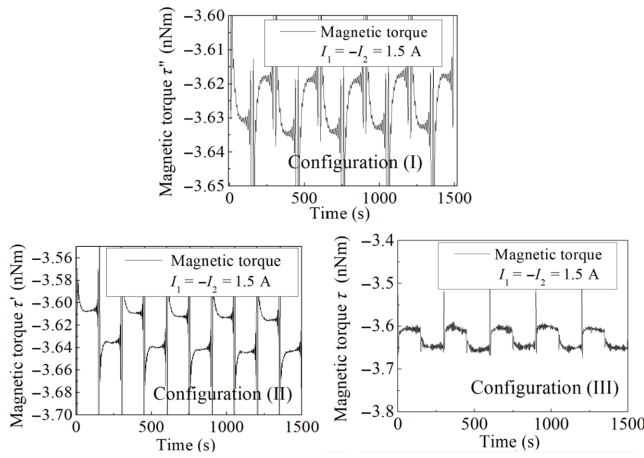| Error term	Error value	Error for m_y (nA m^2)	Error for χ (10^{-6})
Accuracy of capacitive sensor C_n	2×10^{-7} pF/Hz$^{1/2}$	0.59	0.66
Readout noise V_{fn}	2 μV/Hz$^{1/2}$	0.03	0.03
Thermal noise of fiber τ_{th}	5×10^{-14} Nm/Hz$^{1/2}$	0.08	0.09
Calibration error of actuator	$< 1\%$	0.24	0.28
Installation error of magnetic coils	< 50 μm	0.21	0.23
Stability of currents I_1, I_2	1 mA	0.02	0.02

FIG. 8. Curves of the magnetic torques τ, τ', and τ'' that are produced in configurations (I), (II), and (III), respectively. Two magnetic coils are loaded by currents varied periodically as a square wave with a peak-to-peak value of 1.5 A and period of 5 min.

by magnetic gradient. Its variation $\Delta\tau'$ is $(3.83 \pm 0.03) \times 10^{-11}$ Nm. Combining the experimental results from the three configurations, τ, τ', and τ'', from Eqs. (9)–(11), the magnetic susceptibility χ and remanent magnetization can be obtained: $\chi = (9.09 \pm 0.08) \times 10^{-5}$, $m_y = -(31.70 \pm 0.71)$ nA m^2, $m_z = -(126.12 \pm 4.7)$ nA m^2. Using the above method, a series of data are obtained with four different exciting currents of 0.9, 1.2, 1.5, and 1.7 A. Figure 9 shows the results of repeat measurements with different modulation currents. The standard deviations σ_{my} and σ_{χ} are less than 1 nA m^2 and 8×10^{-7}, respectively, which are well below the requirements of LISA and TianQin. The measurement error σ_{mz} is about 5 nA m^2, which is
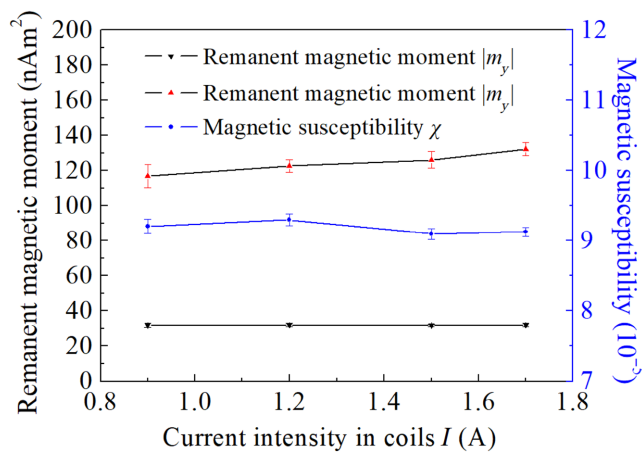

FIG. 9. The results of measurement of remanent magnetization m_y, m_z and magnetic susceptibility χ with different modulation currents. The experimental results of m_y, χ and m_z exhibit very good repeatability in the range of errors, and the values increase with increasing currents.
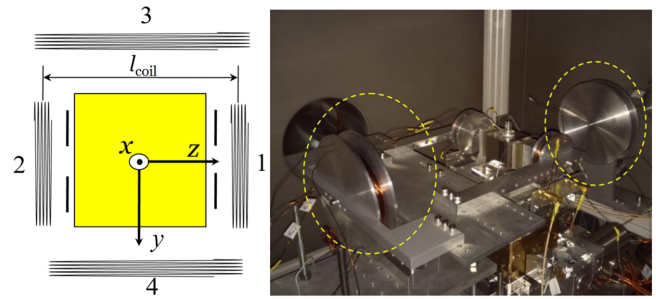

FIG. 10. The installation diagram of magnetic coils. Coils 3 and 4 are designed to counteract the geomagnetic field. Coils 3 and 4 both have the same parameters: a diameter of (5.1 ± 0.1) cm, total turn number of 650, and gap of (41.6 ± 0.1) cm.

larger than σ_{my} because of the relatively low sensitivity and cumulative error of multiple measurements. Certainly, another remanent magnetization m_z also can be measured by rotating the TM 90° for better precision.

IV. ASSESSING THE IMPACT OF THE GEOMAGNETIC FIELD

The major difference between the space environment and the ground environment is the influence of the Earth [26]. If we are to estimate the remanent magnetization of a TM, it is necessary to counteract the influence of the geomagnetic field. So another two coils are added in the apparatus to produce a constant magnetic field that is opposite to the geomagnetic field, as shown in Fig. 10. The component of the geomagnetic field along the y axis is (25.99 ± 0.05) μT measured by a magnetometer. According to our calculation, currents of 0.47 A are loaded in coils 3 and 4 to ensure that the residual magnetic field along the y axis is smaller than 3 μT. In this condition, the remanent magnetization can be obtained in the same way as mentioned for configuration (I). The experimental data show that the remanent magnetization component m_y is $-(29.81 \pm 0.83)$ nA m^2. Comparing experimental results for m_y before and after compensating for the geomagnetic field, the difference of remanent magnetic moment of 2.9 nA m^2 may be derived from the variation of remanent magnetic moment of magnetic impurities existing in the TM. The source of remanent magnetic moment and its variation should be investigated in the future.

V. CONCLUSION AND FUTURE WORK

Magnetic cleanliness is strictly required for the TM of TianQin, and therefore extensive testing for the TM in the laboratory is needed prior to the launch of TianQin. In this paper, an electrostatically controlled torsion pendulum is used to measure the magnetic properties of a TM, and its precision is sufficient to meet the requirements of the Tian-Qin mission. Using a tungsten TM as an example, it is

demonstrated that the standard deviations of the remanent magnetization and susceptibility are better than $1\,\mathrm{nA\,m^2}$ and 8×10^{-7}. Therefore, this facility is able to be a reliable platform for estimating magnetic properties of TMs in other gravitational observatories. At present, our experimental results are based on the assumption of uniform distribution of remanent magnetic moment and magnetic susceptibility. The nonuniform magnetic properties of TMs will be investigated in subsequent work.

[1] W. M. Folkner, P. L. Bender, and R. T. Stebbins, LISA Mission Concept Study Laser Interferometero Space Antenna For the Detection and Observation of Gravitational Wave, JPL Publication 97–16 (1998).

[2] B. Hiscock and R. W. Hellings, Omega: A space gravitational wave midex mission, Bull. Am. Astron. Soc. **29**, 1312 (1997).

[3] J. Luo, L. S. Chen, H. Z. Duan, Y. G. Gong, S. C. Hu, J. H. Ji, Q. Liu, J. W. Mei, V. Milyukov, M. Sazhin, *et al.*, TianQin: A space-borne gravitational wave detector, Class. Quantum Grav. **33**, 035010 (2016).

[4] S. Vitale, The LISA Technology Package on board SMART-2, Architect Final Report (2002).

[5] M. Huller, Ph.D thesis, University of Trento, 2003.

[6] J. Hanson, R. Byer, D. Lauben, S. Williams, B. Shelef, and G. Shelef, ST-7 gravitational reference sensor: Analysis of magnetic noise sources, Class. Quantum Grav. **20**, S109 (2003).

[7] W. Su, Y. Wang, Z. B. Zhou, Y. Z. Bai, Y. Guo, C. Zhou, T. Lee, M. Wang, M. Y. Zhou, H. Yin, *et al.*, Analyses of residual accelerations for TianQin based on the global MHD simulation, Class. Quantum Grav. **37**, 185017 (2020).

[8] A. Hammesfahr, D. Satellitensysteme, P. Bender, A. Brillet, A. M. Cruise, K. Danzmann, F. Fidecaro, W. M. Folkner, J. Hough, P. McNamara, *et al.*, Laser interferometer space antenna: A cornerstone mission for the observation of gravitational waves, ESA-SCI **11**, P63 (2000).

[9] D. Bortoluzzi, C. D. Hoyle, M. Hueller, S. Vitale, G. Heinzel, K. Danzmann, A. Lobo, S. Anza, C. Navau, D. X. Chen, *et al.*, Science Requirements and Top-level Architecture Definition for the LISA Technology Package (LTP) on Board LISA Pathfinder (SMART-2), LISA Technology Package, LTPA-UTN-ScRD (2005).

[10] F. Antonucci, M. Armano, H. Audley, G. Auger, M. Benedetti, P. Binetruy, C. Boatella, J. Bogenstahl, D. Bortoluzzi, P. Bosetti, *et al.*, From laboratory experiments to LISA Pathfinder: Achieving LISA geodesic motion, Class. Quantum Grav. **28**, 094002 (2011).

[11] S. Vitale, *The LISA Pathfinder experiment, oral report in 9th LISA symposium*, Paris, May (2012).

[12] M. Armano, H. Audley, J. Baird, P. Binetruy, M. Born, D. Bortoluzzi, E. Castelli, A. Cavalleri, A. Cesarini, A. M. Cruise, *et al.*, Beyond the Required LISA Free-Fall Performance: New LISA Pathfinder Results Down to 20 Hz, Phys. Rev. Lett. **120**, 061101 (2018).

[13] P. Sarra, S. Legramandi, and C. Clnquepalml, TM FM4 magnetic moment measurement report, LISA Technology Package (2012).

[14] M. Huller, M. Armano, L. Carbone, A. Cavalleri, R. Dolesi, C. D. Hoyle, S. Vitale, and W. J. Weber, Measuring the LISA test mass magnetic properties with a torsion pendulum, Class. Quantum Grav. **22**, S521 (2005).

[15] H. B. Tu, Y. Z. Bai, Z. B. Zhou, Y. R. Liang, and J. Luo, Measurement of magnetic properties of an inertial sensor with a torsion balance, Chin. Phys. Lett. **26**, 040403 (2009).

[16] L. Carbone, A. Cavalleri, R. Dolesi, C. D. Hoyle, M. Hueller, S. Vitale, and W. J. Weber, Achieving Geodetic Motion for LISA Test Masses: Ground Testing Results, Phys. Rev. Lett. **91**, 151101 (2003).

[17] A. Cavalleri, G. Ciani, R. Dolesi, A. Heptonstall, M. Hueller, D. Nicolodi, S. Rowan, D. Tombolato, S. Vitale, P. J. Wass, and W. J. Weber, Increased Brownian Force Noise from Molecular Impacts in a Constrained Volume, Phys. Rev. Lett., **103**, 140601 (2009).

[18] F. Antonucci, A. Cavalleri, R. Dolesi, M. Hueller, D. Nicolodi, H. B. Tu, S. Vitale, and W. J. Weber, Interaction between Stray Electrostatic Fields and a Charged Free-Falling Test Mass, Phys. Rev. Lett. **108**, 181101 (2012).

[19] S. E. Pollack, S. Schlamminger, and J. H. Gundlach, Temporal Extent of Surface Potentials between Closely Spaced Metals, Phys. Rev. Lett. **101**, 071101 (2008).

[20] M. Bassan, A. Cavalleri, M. De Laurentis, F. De Marchi, R. De Rosa, L. Di Fiore, R. Dolesi, N. Finetti, F. Garufi, A. Grado, *et al.*, Approaching Free Fall on Two Degrees of Freedom: Simultaneous Measurement of Residual Force and Torque on a Double Torsion Pendulum, Phys. Rev. Lett. **116**, 051104 (2016).

[21] H. B. Tu, Y. Z. Bai, Z. B. Zhou, L. Liu, L. Cai, and J. Luo, Performance measurements of an inertial sensor with a two-stage controlled torsion pendulum, Class. Quantum Grav. **27**, 205016 (2010).

[22] Z. B. Zhou, L. Liu, H. B. Tu, Y. Z. Bai, and J. Luo, Seismic noise limit for ground-based performance measurements of an inertial sensor using a torsion balance, Class. Quantum Grav. **27**, 175012 (2010).

[23] H. Yin, Y. Z. Bai, M. Hu, L. Liu, J. Luo, D. Y. Tan, H. C. Yeh, and Z. B. Zhou, Measurements of temporal and spatial variation of surface potential using a torsion pendulum and a scanning conducting probe, Phys. Rev. D **90**, 122001 (2014).

[24] M. Hu, Y. Z Bai, Z. B. Zhou, Z. X. Li, and J. Luo, Resonant frequency detection and adjustment method for a capacitive transducer with differential transformer bridge, Rev. Sci. Instrum **85**, 055001 (2014).

[25] W. Tian, S. C. Wu, Z. B. Zhou, S. B. Qu, Y. Z. Bai, and J. Luo, High resolution space quartz-flexure accelerometer based on capacitive sensing and electrostatic control technology, Rev. Sci. Instrum. **83**, 095002 (2012).

[26] E. Willemenot and P. Touboul, On-ground investigation of space accelerometers noise with an electrostatic torsion pendulum, Rev. Sci. Instrum. **71**, 302 (2000).